# Use of Anionic Surfactant Sodium Lauryl Ether Sulfate as a Capping Agent in Metal-Chalcogenide PbS Thin Film Production

E. Yücel*

*Department of Physics, Faculty of Arts and Sciences, Hatay Mustafa Kemal University, 31060 Hatay, Turkey*

          *e-mail:  eyucel@mku.edu.tr

In this paper, nanostructured semiconductor PbS metal-chalcogenide thin films were fabricated by the chemical bath deposition method in a surface active agent environment. The structural, morphological, and optical properties of PbS thin films were characterized by X-ray diffraction, scanning electron microscopy, scanning probe microscope and ultraviolet-visible spectroscopy analyses. These analyses reveal that surfactant sodium lauryl ether sulphate plays a key role in modifying the surface roughness and optical properties of PbS thin films. The average surface roughness decreased from 87.9 to 42.8 nm after adding sodium lauryl ether sulfate to the chemical bath solutions. With the increasing sodium lauryl ether sulfate content, the optical band gaps of the PbS thin films increased from 2.10 to 2.52 eV. Additionally, the optical transmittance value of the 3% sodium lauryl ether sulfate added sample increased by approximately 37% compared to the pure sample.

topics: PbS, chemical bath deposition, surfactant, surface roughness

## 1. Introduction

Chalcogenide is a chemical compound formed by the combination of a chalcogen anion and an electropositive element. The term chalcogenides are used for sulfides, selenides, and tellurides, which belong to the 16 groups of elements of the periodic table [1]. Among the metal-chalcogenide compounds, the lead sulfide (PbS) semiconductor compound has an important place in terms of its properties. We can list these properties as abundance in nature, good chemical stability, high absorption coefficient, high mobility, large exciton Bohr radius, and small band gap [2–4]. PbS is a white crystalline solid. Its relative density is 6.2 g/ml at 25°C and melting point is 1170°C. In addition, PbS is a naturally p-type semiconductor material, and its direct band gap can vary between 0.41 and 2.3 eV [5]. These properties of PbS metal-chalcogenide semiconductor compound make it prominent for solar absorption applications, infrared sensing applications, and gas sensor applications [6–8]. High-quality PbS thin films can be produced using a surfactant [5]. The word surfactant consists of the words surface active agent (surfactant). Surfactants generally have the property of reducing surface tension when dissolved in an aqueous solution [9]. Surfactants can change the morphological structure of thin films [10]. In addition, when the literature is examined, it is seen that surfactants can act as capping agents [11].

In our previous study, PbS thin films are fabricated by the chemical bath deposition (CBD) method using the surfactant cocamidopropyl betaine (CAPB). We obtained that the presence of different amounts of the surfactant CAPB during the PbS deposition process was involved in the formation of decreasing surface roughness. Also, we found that band gaps of the PbS thin films increased from 1.84 to 2.40 eV with increasing of surfactant amount [5]. Nikam et al. [9] have used surfactant polyvinyl alcohol in the deposition of PbS thin films grown by chemical route. They suggested that a small amount of polyvinyl alcohol is useful to get uniform, pinhole-free PbS thin film by chemical bath deposition. Also, they concluded that the band gap of PbS thin films is in the range of 2.28–2.51 eV for polyvinyl alcohol-added PbS thin films. Khan et al. [12] studied the effects of surfactants on the morphology of PbS thin films using sodium dodecyl sulfate (SDS), Tween and Triton X-100. They suggested that Triton X-100 favored rod-like morphology of the as-deposited PbS, while sodium dodecyl sulfate produced spherical shape crystallites predominantly.

PbS nanoparticles can be deposited by different deposition methods, such as chemical bath deposition (CBD), successive ionic layer adsorption and reaction (SILAR), sol–gel, electrodeposition, RF-sputtering, spray pyrolysis etc. [17, 21–25]. Among these production methods, chemical methods such

as CBD, SILAR, sol–gel and spray pyrolysis provide the opportunity of producing thin films in the surfactant medium. The CBD technique, which is one of the chemical production methods, is widely used in the production of metal-chalcogenide thin films by using surfactant [5, 9, 13–15]. The chemical bath deposition method is a simple, safe and low-cost method, and high-quality thin films can be produced using this method [16–20].

In this study, the surfactant sodium lauryl ether sulfate (SLES) was used for the first time in the literature as a capping agent in the production of PbS metal-chalcogenide thin films. PbS thin films were successfully produced by the CBD technique in the presence of different ratios of surfactant. Changes in the surface morphology and optical and structural properties of the PbS thin films produced in the presence of surfactant were investigated. It was observed that the crystal size and surface roughness values of the films decreased with the addition of SLES to the growth solution of PbS thin films. In addition, it was obtained that the optical band gap and transmittance values of the thin films increased with the increase in the amount of SLES in the film growth solution.

## 2. Experimental procedure

In this experiment, first, glass substrates were cleaned in an ultrasonic bath with a sulfuric acid solution, acetone, and deionized water for ten minutes. The surfactant chemical compound was purchased from a local detergent factory. Other chemical compounds were purchased from Merk. PbS metal-chalcogenide thin film production solution was prepared using 0.5 M lead (II) acetate trihydrate $(Pb(CH_3COO)_2 \cdot 3H_2O)$, 1 M thiourea $(NH_2CSNH_2)$, 1 M triethanolamine $(C_6H_{15}NO_3)$ and 1 M tri-sodium citrate $(C_6H_5Na_3O_7)$ reagents. The pH of the film-production solution (with and without surfactant) was adjusted to 12.5 by adding 2 M NaOH. To investigate the effect of surfactant sodium lauryl ether sulfate concentration, 1, 2, and 3% SLES were added to the film growth solutions. The glass substrates were dipped into the growth solution for 18 h under static conditions. Finally, the PbS-coated thin films on the glass surfaces were washed with ultrapure water and air-dried.

For the X-ray diffraction (XRD) characterization of the with and without SLES-mediated PbS thin films, a Rigaku Smart Lab X-ray diffractometer was used. The surface morphologies of all PbS thin films were investigated by using a JEOL 5500/OXFORD Inca-X scanning electron microscopy (SEM). The surface roughness values of all PbS thin films were determined by using a scanning probe microscope (SPM). Optical absorbance and transmittance values of all PbS thin films were measured by using a ultraviolet-visible (UV-Vis) spectrophotometer (Thermo Scientific Evolution 160).

## 3. Results and discussion

### 3.1. Structural properties

X-ray diffraction patterns were obtained for the structural characterization of PbS thin films deposited surfactant-free and surfactant-added. The XRD model confirming the polycrystalline structure of PbS thin films produced with CBD is shown in Fig. 1. The XRD patterns of PbS metal-chalcogenide nanostructured thin films showed no peaks related to elemental lead, other lead sulfides, sulfur, or impurities. Reflection peaks are assigned to planes (111), (200), (220), (311), (222), (400), (331), (420), (422), and (511) at 25.86°, 30.03°, 42.88°, 50.86°, 53.46°, 62.50°, 68.91°, 70.83°, 78.81°, and 84.71°, respectively. These results are in agreement with the standard data of JCPDS (05-0592) data. Comparison of the observed XRD pattern with the standard JCPDS data showed that all the deposited PbS thin films exhibit face-centered cubic structure.

It can be seen from both Fig. 1 and Table I that the (200) diffraction peak intensity decreases as the amount of SLES increases from 1% to 2%, but increases as the amount of SLES increases from 2% to 3%. Also, the (111) diffraction peak intensity decreased as the amount of SLES increased from 1% to 3%. The increase in the diffraction peak intensity of the films indicates an improvement of the crystal quality, while the decrease in the diffraction peak intensity indicates some structural defects caused by the additive surfactant [5]. However, it should be noted that the increased SLES contribution did not significantly reduce the intensity of the (200) and (111) main diffraction peaks of the films.
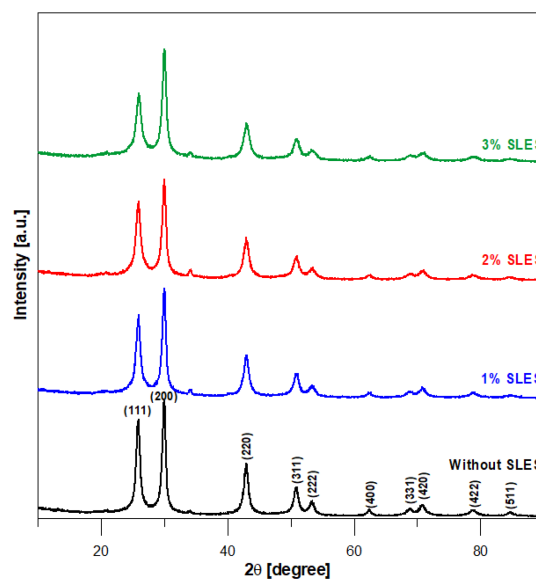


Fig. 1. X-ray diffraction patterns of the PbS films for given SLES concentrations in the growth solutions.

Recorded peak intensity and TC$_{(hkl)}$ values of the PbS thin films as a function of SLES concentrations.

| SLES concentration in | Recorded peak intensity | | TC$_{(hkl)}$ | | | |
|---|---|---|---|---|---|---|
| the growth solution [%] | (200) | (111) | (200) | (111) | (220) | (311) |
| 0 | 3507 | 2951 | 1.30 | 1.22 | 0.73 | 0.42 |
| 1 | 3333 | 2549 | 1.27 | 1.33 | 0.68 | 0.40 |
| 2 | 3069 | 2431 | 1.27 | 1.23 | 0.70 | 0.42 |
| 3 | 3431 | 2132 | 1.12 | 1.29 | 0.66 | 0.41 |

FWHM, crystallite size, thickness, microstrain, dislocation density and band gap energy values of the PbS thin films as a function of SLES concentrations.

| SLES concentration in the growth solution [%] | FWHM [radian] | Crystallite size $D$ [nm] | Thickness [nm] | Microstrain $\varepsilon$ ($\times 10^{-3}$) | Dislocation density $\rho \times 10^{15}$) [m$^{-2}$] | Band gap [eV] |
|---|---|---|---|---|---|---|
| 0 | 0.01169 | 12.81 | 869 | 2.82 | 5.57 | 2.10 ± 0.1 |
| 1 | 0.01280 | 11.71 | 855 | 3.09 | 6.67 | 2.28 ± 0.1 |
| 2 | 0.01309 | 11.45 | 848 | 3.16 | 6.98 | 2.34 ± 0.1 |
| 3 | 0.01367 | 10.96 | 793 | 3.30 | 7.61 | 2.52 ± 0.1 |

The texture coefficient TC$_{(hkl)}$ was used to determine the preferred crystal plane orientations. The texture coefficients of the films were calculated by using the following equation from the XRD data [26]

$$\text{TC}_{(hkl)} = \frac{I_{(hkl)}/I_{0(hkl)}}{N^{-1}\sum\limits_{N} I_{(hkl)}/I_{0(hkl)}}, \qquad (1)$$

where the measured intensity is $I_{(hkl)}$, the standard intensity is $I_{0(hkl)}$ and the number of reflections is $N$. If the TC$_{(hkl)}$ value of a plane is greater than one, that plane is considered a preferential orientation. The texture coefficient values of the (200) and (111) planes are given in Table I. As shown in Table I, it can be interpreted that planes (200) and (111) are preferential planes and are superior to other orientations with increased SLES amount.

The crystallite size ($D$) of PbS metal-chalcogenide thin films is estimated with the Scherrer's formula by using a peak width of (200) [27],

$$D = \frac{0.94\lambda}{\beta \cos(\theta)}, \qquad (2)$$

where $\lambda$ is a wavelength and is equal to 1.5406 Å, $\beta$ is the full width at half-maximum (FWHM), and $\theta$ is the Bragg angle. FWHM and crystallite size values calculated depending on the amount of SLES are given in Table II. Depending on the increasing SLES additive amount, it was obtained that while the FWHM values increased, the crystallite size values decreased. The conditions of the production of metal-chalcogenide thin films have a decisive role in the crystallite size of these films. Surfactants have been reported in the literature to act as capping agents. The reduction in crystallite size of the thin films may be related

to the capping agent. The presence of a capping agent in the growth solution of the thin films can restrict particle growth [5, 28, 29]. Table II shows that the thickness of the PbS films decreases with increasing SLES adding ratio. The decrease in the film thickness may be due to the slowing of the film adhesion process on the glass substrate with the increase in the amount of SLES in the growth solution.

Microstrain ($\varepsilon$) and dislocation density ($\rho$) of the PbS metal-chalcogenide thin films were calculated using the respective equations [30]

$$\varepsilon = \frac{\beta}{4}\cos(\theta), \qquad (3)$$

$$\rho = \frac{15\varepsilon}{aD}, \qquad (4)$$

where $a$ is the lattice parameter. The calculated values of dislocation density and microstrain of the thin film samples are given in Table II. As can be seen there, the microstrain values of the PbS thin films increased from $2.82 \times 10^{-3}$ to $3.30 \times 10^{-3}$, while the dislocation density values increased from $5.57 \times 10^{15}$ to $7.61 \times 10^{15}$ m$^{-2}$. If the crystallite size decreases in the PbS metal-chalcogenide structures, the grain boundaries increase and lattice defects increase accordingly. As a result, the values of dislocation density and microstrain of the PbS metal-chalcogenide structures may increase [31].

### 3.2. Morphological properties

The surface structures of nanostructured thin films play an important role in the optical properties of thin films. The surface morphology of thin films can affect the efficiency of photovoltaic devices. The surface structures of the synthesized PbS

TABLE III

The profile roughness ($R_a$, $R_q$) and the area roughness ($S_a$, $S_q$) parameters of the PbS thin films prepared with different SLES concentrations.

| SLES concentration in the growth solution [%] | Mean roughness $S_a$ [nm] | RMS roughness $S_q$ [nm] | Average surface roughness $R_a$ [nm] | RMS roughness $R_q$ [nm] |
|---|---|---|---|---|
| 0 | 89.3 | 145.9 | 87.9 | 143.0 |
| 1 | 72.7 | 107.5 | 71.1 | 105.3 |
| 2 | 55.3 | 80.8 | 54.7 | 79.6 |
| 3 | 43.6 | 64.4 | 42.8 | 63.6 |
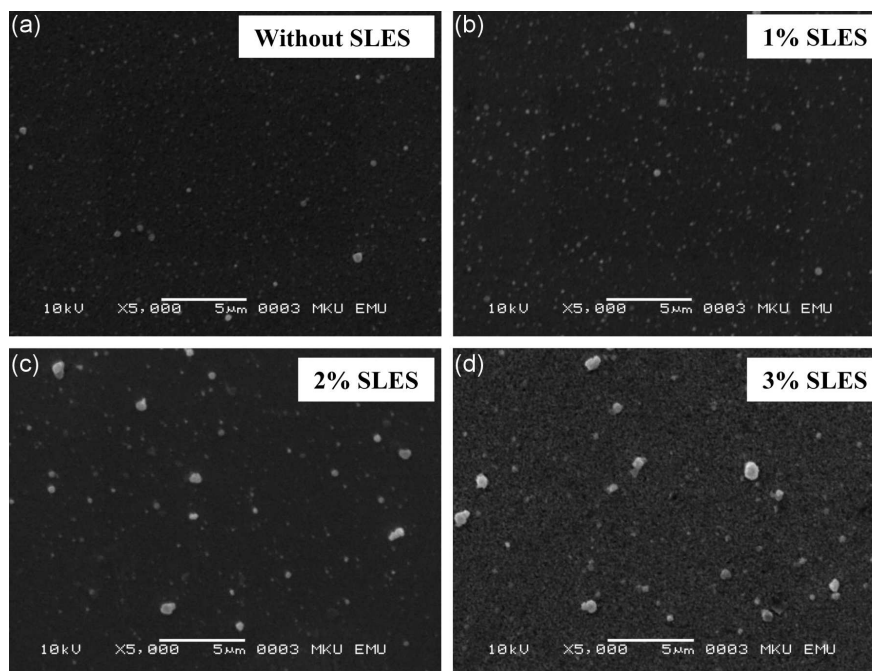


Fig. 2. Scanning electron microscopy images of the PbS films as a function of SLES concentrations in the growth solutions.

metal-chalcogenide thin films were investigated using SEM and SPM analyses. SEM images of the PbS thin films deposited surfactant-free and SLES-added with various ratios are shown in Fig. 2.

In general, it can be seen from the SEM photographs that all PbS thin films have a homogeneous and dense surface structure. SPM analysis is one of the alternative methods of analyzing the surface morphology of thin films and thin coatings [5, 32, 33]. Three-dimensional (3D) SPM images of PbS thin films produced with and without surfactant are shown in Fig. 3. The roughness values ($R_a$, $R_q$, $S_a$, $S_q$) of the PbS metal-chalcogenide films were calculated by SPM analysis. The roughness values of the samples are given in Table III.

When one examines Fig. 3 and Table III, it is seen that the PbS thin film produced without surfactant has a rougher surface than the thin films fabricated with SLES. With the increase in the amount of surfactant SLES in the growth solution, the roughness values $R_a$, $R_q$, $S_a$, $S_q$ of the samples decreased.

These results confirmed that the surfactant SLES has a significant effect on the surface roughness of PbS metal-chalcogenide thin films. At the same time, these results indicate that the roughness of thin films can be controlled by choosing an appropriate SLES additive ratio.

### 3.3. Optical properties

The optical absorbance spectra of the samples are given in Fig. 4. The absorption spectrum shows that all produced samples are active in the UV and visible regions. For all films, it was obtained that the absorption was higher in the UV and visible regions, while the absorption was low in the infrared (IR) region. This result is compatible with the literature. Similar results regarding optical absorbance analysis studies of PbS thin films have been presented in the literature [34–36]. As seen in Fig. 4, the spectra show an increasing absorbance from the near-infrared (NIR) region to the visible region.

**Without SLES**

(a)

**1% SLES**

(b)

**2% SLES**

(c)

**3% SLES**

(d)
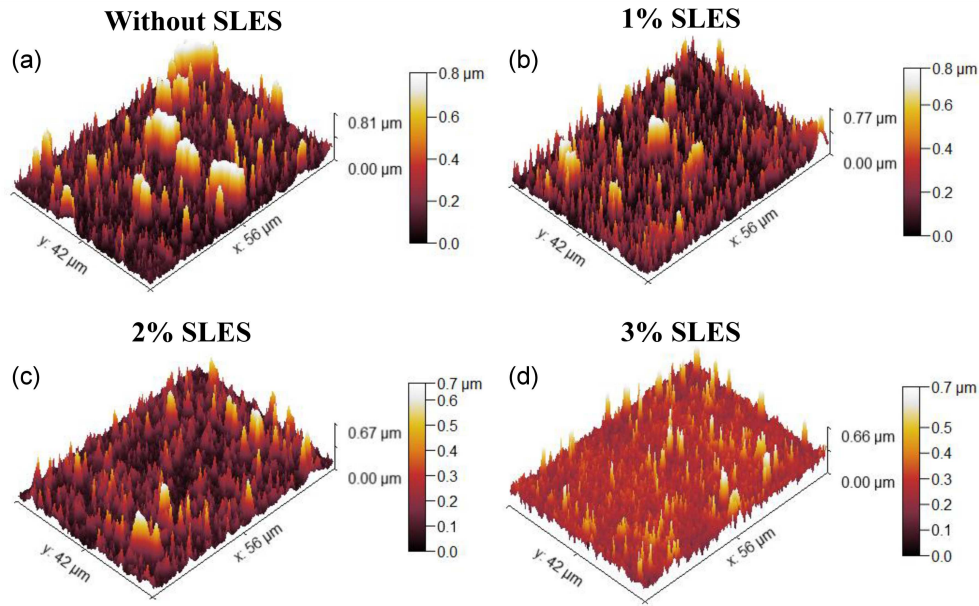
Fig. 3. SPM images of the PbS films as a function of SLES concentrations in the growth solutions (a–d).
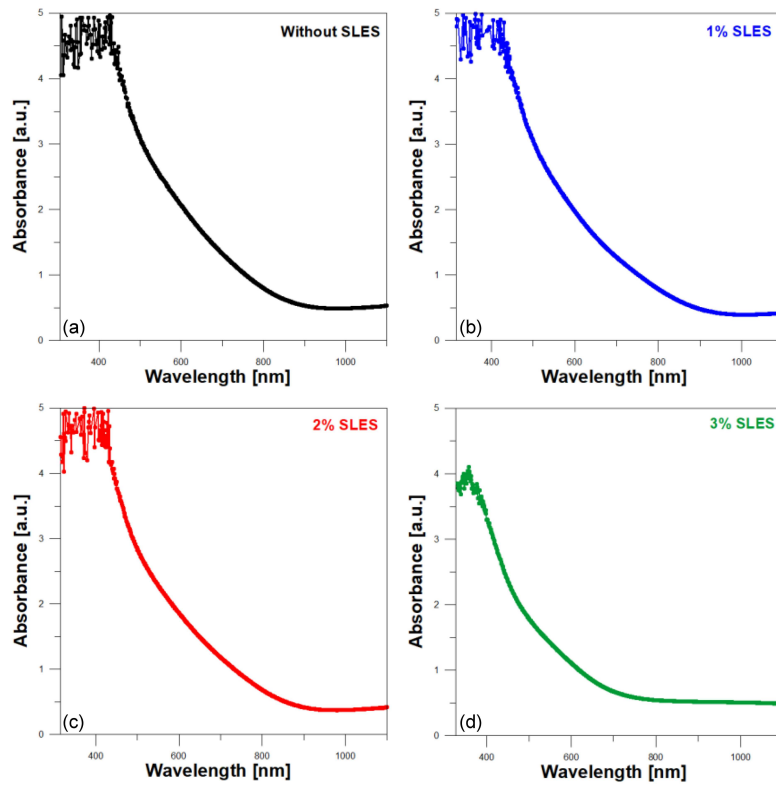
Fig. 4. UV-Vis absorbance spectra of the PbS films at different SLES concentrations (a–d).

The increased absorption may be due to the transition of electrons from the valence band to the conduction band [34]. It can also be seen in Fig. 4 that the absorption edge shifts towards a lower wavelength as the amount of SLES in the growth solution of PbS thin films increases. This blue shift at the absorption edge indicates an increase in the optical band gap values of PbS thin films [36]. It was found that the 1% and 2% SLES additives did not significantly reduce the absorbance of the films in the UV and Vis wavelength regions. It was found that the absorption edges of all thin film samples were not sharp. This is an expected result for an ideal semiconductor.
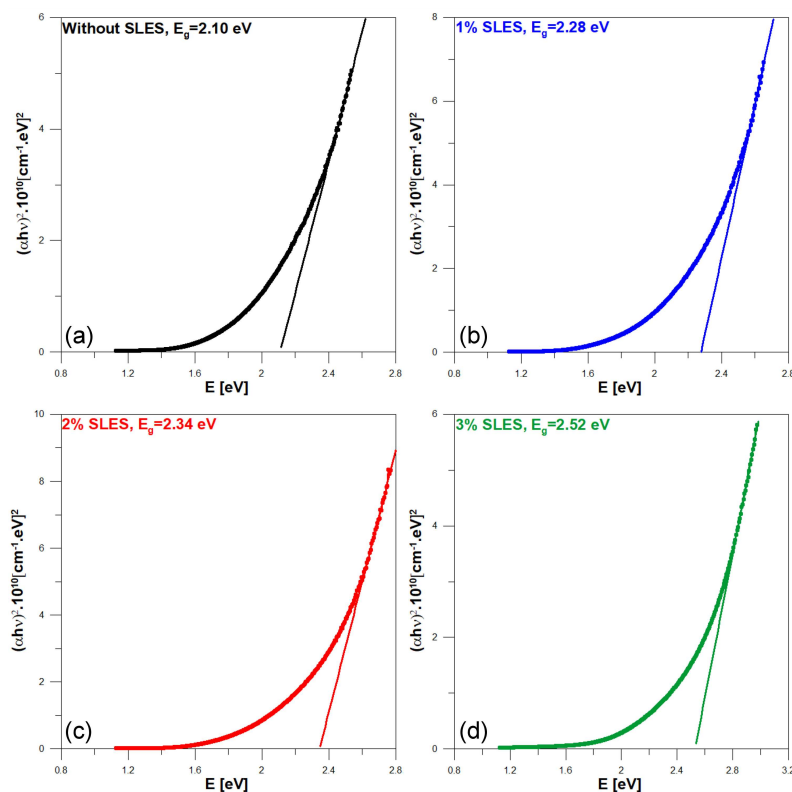
Fig. 5. Optical band gap spectra of the PbS films at different SLES concentrations (a–d).

The following classical Tauc absorption equation was used to calculate the optical band gap values of PbS thin films [37],

$$(\alpha h\nu) = C\left(h\nu - E_g\right)^n, \tag{5}$$

Now, the $E_g$ values of PbS thin films were calculated from the measured absorbance data. The optical band gap graphs of $(\alpha h\nu)^2$ versus $h\nu$ are shown in Fig. 5. The values of the band gap were obtained to be 2.10, 2.28, 2.34, and 2.52 eV for 0, 1, 2, and 3% SLES added samples, respectively. The lowest optical band gap was obtained for the pure PbS thin film sample.

This result shows that the optical band gap values of the PbS thin films produced with the support of surfactant SLES increased. Also, the relationship between the optical band gap and the crystal size of the thin film samples is shown in Fig. 6. As seen in Fig. 6, the crystallite size of the samples decreased while the optical band gap increased with the SLES addition. This result can be explained by the quantum confinement effect. The semiconductor PbS compound has a big exciton Bohr diameter ($\simeq 36$ nm). If the particle size of the semiconductor compound is smaller than the Bohr exciton diameter, the quantum confinement effect is observed [5, 19, 20, 26].

Figure 7 shows the transmittance graphs of PbS metal-chalcogenide thin films fabricated surfactant-free and surfactant-added. Optical transmittance values were obtained as $\sim 33\%$, $\sim 42\%$, $\sim 43\%$
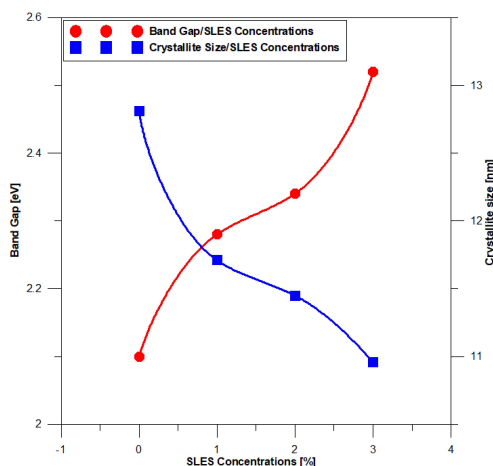


Fig. 6. Band gap and crystallite size variation as a function of SLES concentrations in the growth solutions.

and $\sim 45\%$ for 0, 1, 2 and 3% SLES added thin films, respectively. High optical transmittance in the IR wavelength region was obtained for all thin film samples. It was observed that the optical transmittance value of the 3% SLES added sample increased by approximately 37% compared to the pure sample. In addition, according to Fig. 7, the shift of the absorption edge of the samples to shorter wavelengths with the SLES addition indicates that the
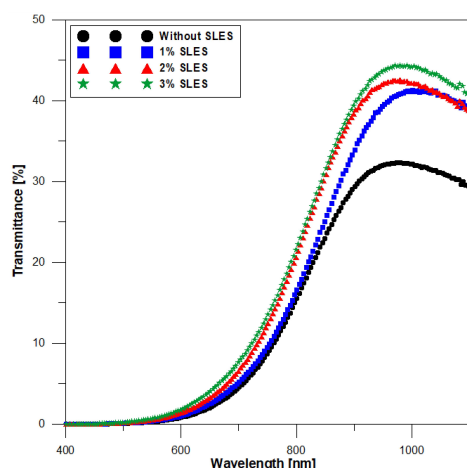
Fig. 7. UV-Vis transmittance spectra of the PbS films at different SLES concentrations.

optical band gap of the PbS films increases. All optical examination results indicate that the adding ratio of the surfactant SLES can determine the optical properties of PbS metal chalcogenide thin films.

## 4. Conclusions

Metal-chalcogenide PbS polycrystalline thin films were successfully grown using surfactant with a chemical bath deposition method. Variations in the structural, morphological, and optical properties of PbS thin films after adding surfactant SLES in the growth bath were investigated. By XRD analysis, it was obtained that the PbS thin films crystallize well in a face-centered cubic structure with a preferential orientation along the (200) and (111) planes. The crystallite size of the PbS thin films decreased with the addition of SLES. According to the SPM results, the roughness values ($R_a$, $R_q$, $S_a$, $S_q$) of the PbS thin films decreased with increasing SLES amount in the growth solution. Based on the optical measurements, the absorption of all PbS thin films increased from the near-infrared (NIR) region to the visible (Vis) region. The band gap and transmittance values of the samples increased with the increasing surfactant SLES content. In general, the addition of surfactant SLES as a capping agent positively affected the surface morphology, and optical and structural properties of PbS thin films.

## References

[1] E. Yücel, Y. Yücel, M. Durak, *J. Alloy Compd.* **664**, 530 (2016).

[2] J. Gaur, H.K. Sharma, S.K. Sharma, B.P. Singh, *Indian J. Pure Appl. Phys.* **57**, 709 (2019).

[3] K. Paulraj, S. Ramaswamy, M. Shkir, I.S. Yahia, M.S. Hamdy, S. AlFaify, *J. Mater. Sci. Mater. Electron.* **31**, 1817 (2020).

[4] M. Xing, Y. Wei, R. Wang, Z. Zhang, *Solar Energy* **213**, 53 (2021).

[5] E. Yücel, *Superlattice Microst.* **135**, 106287 (2019).

[6] A.E. Adeoye, E. Ajenifuja, S.O. Alayande, E.D. Ogunmola, O.A. Adeyemi, A.Y. Fasasi, *SN Appl. Sci.* **2**, 1560 (2020).

[7] L. Qin, S. Wu, J.G. Wang, Q. Li, C. Yuan, Z. Wang, J. Wang, Z. Hu, L. Wang, Q. Wang, *Infrared Phys. Technol.* **121**, 104033 (2022).

[8] T.V. Beatriceveena, E. Prabhu, A.S.R. Murthy, V. Jayaraman, K.I. Gnanasekar, *Appl. Surf. Sci.* **456**, 430 (2018).

[9] S.S. Nikam, M.P. Suryawanshi, M.A. Gaikwad, J.H. Kim, A.V. Moholkar, *J. Mater. Sci. Mater. Electron.* **28**, 5165 (2017).

[10] N.D. Desai, P.N. Bhosale, *Mater. Today Proc.* **43**, 2730 (2021).

[11] G. Yıldırım, E. Yücel, *J. Mater. Sci. Mater. Electron.* **33**, 19057 (2022).

[12] M.D. Khan, S. Hameed, N. Haider, A. Afzal, M.C. Sportelli, N. Cioffi, M.A. Malik, J. Akhtar, *Mat. Sci. Semicon. Proc.* **46**, 39 (2016).

[13] I. Ammar, A. Gassoumi, A. Akkari, F. Delpech, S. Ammar, N. Turki-Kamoun, *Eur. Phys. J. Plus* **134**, 505 (2019).

[14] S.A. Vanalakar, S.S. Mali, E.A. Jo, J.Y. Kim, J.H. Kim, P.S. Patil, *Solid State Sci.* **36**, 4 (2014).

[15] W.G.C. Kumarage, R.P. Wijesundera, V.A. Seneviratne, C.P. Jayalath, T. Varga, M.I. Nandasiri, B.S. Dassanayak, *Mater. Chem. Phys.* **200**, 1 (2017).

[16] S. Tec-Yam, J. Rojas, V. Rejón, A.I. Oliva, *Mater. Chem. Phys.* **136**, 386 (2012).

[17] E. Yucel, Y. Yucel, B. Beleli, *J. Alloy Compd.* **642**, 63 (2015).

[18] T. Tohidi, K. Jamshidi-Ghaleh, A. Namdar, R. Abdi-Ghaleh, *Mat. Sci. Semicon. Proc.* **25**, 197 (2014).

[19] E. Yücel, Y. Yücel, *Optik* **142**, 82 (2017).

[20] E. Yücel, Y. Yücel, *Ceram. Int.* **43**, 407 (2017).

[21] E. Yücel, Y. Yücel, B. Beleli, *J. Cryst. Growth* **422**, 1 (2015).

[22] A.I. Nicoara, M. Eftimie, M. Elisa, I.C. Vasiliu, C. Bartha, M. Enculescu, M. Filipescu, C.E. Aguado, D. Lopez, B.A. Sava, M. Oane, *Nanomaterials* **12**, 3006 (2022).

[23] A. Aghassi, M. Jafarian, I. Danaee, F. Gobal, M.G. Mahjani, *J. Electroanal. Chem.*, **661**, 265 (2011).

[24] J. Gaur, H.K. Sharma, S.K Sharma, B.P. Singh, *Indian J. Pure Appl. Phys.* **57**, 709 (2019).

[25] SR Rosario, I Kulandaisamy, KDA Kumar, K Ramesh, HA Ibrahium, NS Awwad, *Int. J. Energy Res.* **44**, 1 (2020).

[26] Y. Yücel, E. Yücel, *Optik* **164**, 263 (2018).

[27] E. Yücel, Y. Yücel, D. Gökhan, *Appl. Surf. Sci.* **351**, 904 (2015).

[28] C.K. Latha, M. Raghasudha, Y. Aparna, M. Ramchander, D. Ravinder, K. Jaipal, P. Veerasomaiah, D. Shridhar, *Mater. Res.* **20**, 256 (2017).

[29] Y. Yan, K-bin. Chen, H-ran. Lı, W. Hong, X-bin. Hu, Z. Xu, *T. Nonferr. Metal Soc.* **24**, 3732 (2014).

[30] E. Yücel, S. Kahraman, H.S. Güder, *Mater. Res. Bull.* **68**, 227 (2015).

[31] L. Zhang, Y. Xiang, *J. Mech. Phys. Solids* **117**, 157 (2018).

[32] T. Liu, C. Li, Q. Li, L. Li, F. Xia, H. Xing, C. Ma, *Int. J. Electrochem. Sci.* **16**, 151028 (2021).

[33] K. Shimizu, Y. Uozaki, K. Nozaki, M. Uenaka, H. Terauchi, I. Takahashi, *J. Am. Oil Chem. Soc.* **90**, 1439 (2013).

[34] T. L. Remadevi, K. C. Preetha, *J. Mater. Sci. Mater. Electron.* **23**, 2017 (2012).

[35] Y. Wang, J. Xia, X. Li, F. Ru, X. Chen, Z. Hua, R. Shao, X. Wang, W. Zhang, C.S. Lee, X. Meng, *Nano Res.* **15**, 5402 (2022).

[36] Z.K. Heiba, M.B. Mohamed, A.M. Elnaggar, A. Badawi, H. Elshimy, *J. Mater. Sci. Mater. Electron.* **33**, 23270 (2022).

[37] E. Yücel, Y. Yücel, *J. Indian Chem. Soc.* **99**, 100706 (2022).